Title

Design of a Compact Actuation and Control System for Flexible Medical Robots

Journal

IEEE Robotics and Automation Letters, 2(3)

ISSN

2377-3766

Authors

Morimoto, Tania K
Hawkes, Elliot Wright
Okamura, Allison M

Publication Date

2017-07-01

DOI

10.1109/lra.2017.2676240

Peer reviewed

HHS Public Access

Author manuscript

IEEE Robot Autom Lett. Author manuscript; available in PMC 2018 June 01.

Published in final edited form as:

IEEE Robot Autom Lett. 2017 July ; 2(3): 1579–1585. doi:10.1109/LRA.2017.2676240.

Design of a Compact Actuation and Control System for Flexible Medical Robots

Tania K. Morimoto,
Department of Mechanical Engineering, Stanford University, Stanford, CA 94035 USA

Elliot Wright Hawkes, and
Department of Mechanical Engineering, Stanford University, Stanford, CA 94035 USA and also with the Department of Mechanical Engineering, University of California, Santa Barbara, CA 93106 USA

Allison M. Okamura
Department of Mechanical Engineering, Stanford University, Stanford, CA 94035 USA

Abstract

Flexible medical robots can improve surgical procedures by decreasing invasiveness and increasing accessibility within the body. Using preoperative images, these robots can be designed to optimize a procedure for a particular patient. To minimize invasiveness and maximize biocompatibility, the actuation units of flexible medical robots should be placed fully outside the patient's body. In this letter, we present a novel, compact, lightweight, modular actuation, and control system for driving a class of these flexible robots, known as concentric tube robots. A key feature of the design is the use of three-dimensional printed waffle gears to enable compact control of two degrees of freedom within each module. We measure the precision and accuracy of a single actuation module and demonstrate the ability of an integrated set of three actuation modules to control six degrees of freedom. The integrated system drives a three-tube concentric tube robot to reach a final tip position that is on average less than 2 mm from a given target. In addition, we show a handheld manifestation of the device and present its potential applications.

Index Terms

Mechanism design; medical robots and systems; surgical robotics: steerable catheters/needles

I. INTRODUCTION

Flexible medical robots, including steerable needles and concentric tube robots, offer enhanced dexterity and manipulation in constrained environments. The workspace, dexterity, and size of these robots [1], [2] depend on parameters including the lengths, curvatures, diameters, and material properties, which can be adjusted to build a robot with characteristics designed on a patient- and procedure-specific basis. Optimizing the design for a specific patient could lead to improved effectiveness and efficiency of procedures. This patient-specific design process could help specialized patient groups, particularly pediatric and obese patients, since current systems are inadequate for their anatomy, which differs from the general population. An accurate and reliable actuation and control system is

required to drive these flexible medical robots. For procedures that require highly curved paths and access deep within the body, these actuation systems can become large, complex, and expensive due to the need to control numerous degrees of freedom. Our particular clinical application is nonlinear renal access to kidney stones in pediatric patients [3], [4]. We propose the use of a compact, lightweight, modular actuation system, shown in Fig. 1, that can be adjusted on a patient-specific basis for controlling these robots.

A. Background

1) Flexible Medical Robots—A large class of dexterous continuum manipulators have been developed for use in surgery and interventional radiology. These include catheters, flexible needles, laparoscopic tools, endoscopes, and concentric tube robots [5]. Actuation, sensing, and control of these robots differ from those of traditional serial manipulators because the robot configuration cannot be defined in closed form by the actuator states, due to their inherent compliance. The focus of this work is on a subset of this class of robots, known as concentric tube robots. However, the proposed system could be used for any flexible robot that requires rotational and translational actuation.

Concentric tube robots consist of a set of hollow, pre-curved elastic tubes that nest concentrically [6], [7]. Because of the elastic interaction between the curvatures of the tubes, inserting and rotating them with respect to one another causes the robot to bend and change shape. Rather than relying on tissue forces or external wires, concentric tube robots derive bending actuation from elastic energy stored in their backbone, enabling smaller and more dexterous designs compared to traditional surgical tools. Adding more independently controlled tubes increases the dexterity of this modular robot.

2) Previous Actuation Unit Designs—The earliest papers on continuum robots used manual actuation [6] or provided little detail of the actuation system design [7]. More recently, researchers have designed various actuation units in order to meet a particular need. For example, the focus of [8], [9] was to develop multi-arm systems for endonasal surgery. The choices for the number of degrees of freedom, motor forces and velocities, and overall travel lengths were made in order to optimize the design for this specific procedure. Other researchers designed MRI-compatible devices that required the use of alternative actuators such as piezoelectric motors [10] and pneumatic cylinders [11]. Another focus has been sterilizability, and both a manual autoclavable system [12] as well as a robotic autoclavable system [13] have been presented. In contrast, a disposable device [14] was designed to be simple and inexpensive.

B. Contributions

Current systems tend to fall under one of two categories —very large but capable of controlling many degrees of freedom, or smaller but capable of controlling only a limited number of degrees of freedom. The need for a compact, lightweight actuation system that does not compromise the number of degrees of freedom motivates our work. Our contributions are as follows. (1) We present a novel actuation system with a drive mechanism that allows for a compact, handheld design. During a procedure, the actuation system can be mounted on an arm or table or held by the doctor, and the small size of the

proposed system is important for easy maneuverability. The compactness and simplicity of the design also increases the feasibility of multi-arm systems in the future. (2) The system is a modular assembly suitable for use in a patient-specific design process. In addition to optimizing the design of the concentric tubes for a specific patient and procedure [3], [4], the components of the actuation and control system used can be selected on a personalized basis.

II. System Design

A. Mechanical Design

Each module of the system is designed to hold a single concentric tube or other flexible medical device, and drives both its translation and rotation using gear-based actuation. There are many linear drive mechanisms available. For example, friction-drive and capstan-drive both offer low backlash but can slip. Leadscrews and ballscrews offer high precision and accuracy [15] but lead to a bulky design since they must either be mounted side-by-side or stacked one after another but cannot nest. Our selection of a drive mechanism considered the need for a minimum of three independent translational degrees of freedom.

1) Design Concept—The mechanism that enables compact actuation of two degrees of freedom for each tube (Fig. 1) is based on a 3D printed roller gear that has teeth in both the radial and axial directions, similar to [16], [17]. The result is a grid or waffle-like pattern as shown in a CAD rendering in the inset image of Fig. 2. By actuating one of the two spur gears that are oriented orthogonal to one another (Fig. 2), the roller gear can be either translated or rotated. When the translation spur gear is actuated, its teeth interact with the axial teeth of the roller gear, causing the roller gear to be inserted or retracted, as shown in Fig. 3(a). Because of the 90° offset between the translation and rotation spur gears as well as the teeth spacing, the roller gear is free to slide without interference from the rotation spur gear. Similarly, when the rotation spur gear is actuated, its teeth interact with the radial teeth of the roller gear, causing the roller gear to rotate about its axis, as shown in Fig. 3(b).

Despite the backlash inherent in a gear-based actuation mechanism, the use of the waffle-like pattern allows for a compact design because each roller gear can align axially and nest inside the previous one. In addition, this design concept enables the transmission to be integrated into the tubes themselves, by fabricating the gearing pattern directly onto the distal bodies of the tubes. While the presented version includes the gearing as a separate body, the concept allows for a future device (described in Section V) that is only slightly larger than the tubes themselves.

The distal end of each roller gear has a split clamp that enables easy mounting of a concentric tube. The roller gear is hollow along its entire length so that multiple roller gears, and therefore concentric tubes, can nest one inside the next. This nesting behavior is an important feature of concentric tube robots, where each robot consists of a series of hollow, precurved tubes that fit inside each other. Each actuation unit controls both degrees of freedom of a single concentric tube, and these units can easily be connected and disconnected depending on the number of tubes that must be controlled for a given application.

The described actuation mechanism, the modular design, and 3D printing technologies enable the overall footprint to be more compact and lightweight than the standard lead screw designs [8]. For example, a system that can drive three concentric tube robots is 17.5″ × 3.5″ × 4″ and weighs less than 490 g. If fewer concentric tubes are needed for a given application, units can be removed, further reducing the overall footprint and weight.

2) Design Features—The base of each actuation unit is made from laser-cut acrylic. Four suction cups are screwed into the bottom of each, allowing easy mounting during testing. In addition, tubes surrounding the proximal end of each roller gear help maintain axial alignment. Each unit also has features that enable quick connections of multiple units to one another as shown in Fig. 4(a). The distal end of each base has male alignment features that fit with the corresponding female features on the proximal end of the subsequent unit. In addition to these male/female connectors, each roller gear has a distinct proximal (front) and distal (back) end, as shown in Fig. 2. This asymmetry also ensures that units can only be joined such that the mounted tubes are all facing the proximal end. The module attachment bars can swivel into place and are easily connected to the subsequent unit with thumb screws as shown in Fig. 4(b). This modularity ensures access to the tube mount, enabling easy attachment of the base of each concentric tube to its respective roller gear. These features also allow for attaching and detaching of the necessary number of units depending on the particular patient and procedure.

The motors are brushed DC Micro Metal motors with a gear ratio of 298:1. The motors were chosen for their small size (10 × 12 × 26 mm), high torque (494 mNm in stall), and low cost ($18.95) compared to previous designs [8], [9]. Each motor is also equipped with a 12 count per revolution quadrature encoder, which is attached to the extended back shaft of the motor, and results in 3576 counts per revolution of the gearbox output shaft.

The gears are 3D printed with plastic (VisiJet M3 Crystal), and their specific dimensions, gear ratios, etc. can be altered based on application needs. For translation to a clinical setting, future versions can be machined out of plastic or metal. Although this entire actuation system remains outside the patient's body during a procedure, the parts would be autoclaved in order to ensure that the concentric tubes remain sterilized as they are attached to the system.

The specifics of the gear designs presented here are shown in Table I. The gear ratios are r_{trans}/r_{roll} (the ratio between the translational spur gear and roller gear) and r_{rot}/r_{roll} (the ratio between the rotational spur gear and roller gear). The selection of these ratios offers another design choice for tuning the overall ratio between motor output torque and concentric tube robot insertion forces and torques.

The number and size of the teeth on each gear is another important design choice. On one end of the spectrum, the maximum tooth size is limited by the diameter of the bearing of the spur gears or by the diameter of the inner channel of the roller gear. In addition, a very small number of these large teeth results in higher backlash. On the other end of the spectrum, the minimum tooth size is limited by the resolution of the 3D printer. Printer accuracy limitations result in a larger percent error for smaller teeth, resulting in reduced meshing and

inefficiency. Smaller teeth are also more fragile and prone to breaking if high loads are unevenly distributed among the teeth.

Finally, the translation distance of each module, which is determined by the length of the roller gear, is a critical feature. The necessary distances are determined by how far the concentric tube robot must be inserted into the body for the given application, and the upper bound on the length of a given roller gear is determined by the print bed size of the 3D printer used. Although making each roller gear as long as possible enables use in a wider range of applications, it also increases the distance between the point at which the tube is grasped and the point at which it enters the body, therefore increasing torsional windup of a concentric tube robot [18].

B. Control

An Arduino Mega is used to control the actuation system. The motors are driven with L298 H-bridge chips, and their position is measured with the quadrature encoders described in Section II-A, which have 3576 counts per revolution of the gearbox output shaft. Position control is implemented on each motor using a simple proportional-integral controller. Conversion from encoder position to distance or angle traveled is performed using the number of encoder counts per revolution of the gearbox output shaft, the gear ratios, and the spur gear circumference (for translation) or degrees per revolution (for rotation).

The control scheme must maintain position control on the unit holding the outermost tube while the internal tube is inserted or retracted. Because of the friction between tubes, translating one tube may result in unwanted coupling between that tube and the one nested around it. Position control was implemented on the outermost tube, in order to ensure that it maintains its current position and opposes this coupling force. Coupling during rotation was not found to be an issue for the particular concentric tube sets we tried. However, the same algorithms could be used on this degree of freedom as well if it proves to be an issue in the future.

III. Precision and Accuracy of Actuation and Control System

In order to test the precision and accuracy of the actuation system, two experiments were performed. The first experiment was designed to measure the amount of backlash in each degree of freedom, and the second was designed to illustrate the performance of the system under various loads and torques.

A. Backlash Experiments

The backlash in each degree of freedom was measured using an Ascension Technology Corporation six-degree-of-freedom tracking sensor and electromagnetic tracking unit (root mean square error of 1.4 mm and 0.5°) [19]. The sensor was secured inside the roller gear being tested. The initial position of the roller gear was set such that an edge of one tooth was in contact with the edge of a tooth of the corresponding spur gear, as shown in Fig. 5(a). The roller gear was then manually moved (translated or rotated depending on the degree of freedom being tested) until the edge of the next tooth on the roller gear came in contact with

the opposite edge of the tooth on the spur gear, as shown in Fig. 5(b), and the roller gear could no longer be manually moved.

Translation and rotation tests were each performed five times for all of the actuation units. The mean and standard deviation are shown in Fig. 6. For each degree of freedom, the backlash was relatively consistent across all units, and the values represent the backlash of the overall device including the highly-geared motors. Although the mean values seem small, we subsequently test the device under various loads to ensure the backlash will not affect performance or accuracy.

B. Accuracy Experiments

Two different sets of experiments were performed in order to measure the accuracy of the device under different loading conditions for both translation and rotation. In both sets of experiments, a single actuation unit was tested, and a proportional-integral controller, as described in Section II-B, was used for each motor. The controller gains for the two degrees of freedom were not identical, resulting in translational or rotational errors that could be positive or negative depending on the gains.

1) Translation—In order to simulate various loading conditions for the translational case, the actuation unit was placed inline with a plastic syringe as shown in Fig. 7. The barrel of the syringe was secured in place, while the plunger was attached to the back of an ATI Industrial Automation Mini 45 force/torque sensor (resolution of 0.125 N and 0.00133 Nm). A rod with an acrylic end plate was used to offset the force/torque sensor from the EM sensor, which was fixed inside the back end of the roller gear and used to measure its position, in order to avoid interference with the EM tracker. During the experiments, an airline was attached to syringe in order to vary the amount of pressure, and therefore load, that the actuation unit needed to overcome.

For each of the four loads shown in Fig. 8, we commanded an insertion of 15 mm and measured the corresponding position and force. The load was determined by averaging the steady state force along the z-axis of the force sensor. As shown in Fig. 8, the average error during the 15 mm insertion was less than 0.5 mm in all cases. Based on a worst-case error of 0.7 mm in both directions, we estimate a maximum hysteresis of the system of 1.4 mm using only low-level position control for each motor. However, with additional feedback control using tip position, this repeatability would be improved further.

2) Rotation—In order to generate various torsional loads, a torsion spring fixture, comprised of two parts, was attached to the actuation unit as shown in Fig. 9. One part of the fixture is attached to the force/torque sensor which is mounted rigidly in place. The other part of the fixture is rigidly mounted with respect to the unit being tested, but is free to rotate with respect to the other part of the spring fixture. As the actuation unit is commanded to rotate against the torque of the spring, the force/torque sensor measures this torque.

To create different torque values, the device was commanded to rotate 15°, 30°, 60°, and 75°. Larger displacement values correspond to larger torsional loads. The error between the actual angle and the commanded angle is calculated based on the angle change measured

using the EM tracker, and the results are shown in Fig. 8. The mean error values for all loads are under 1.5°, even for loads larger than predicted distributed frictional forces [20].

IV. Targeting Experiments With Concentric Tubes

In order to demonstrate the capabilities of the proposed actuation and control system, we drove a set of three Nitinol concentric tubes to various target locations.

A. Experimental Setup

The parameters of the Nitinol tubes used in these experiments are shown in Table II. The curvatures were formed by first laser cutting two identical jigs with the desired constant curvature segments. The straight pieces of Nitinol were then placed inside one jig and clamped closed using the other jig. A power supply was used as in [21] to heat the Nitinol tube to approximately 450 °F as measured with a Fluke Multimeter temperature probe. After cooling, the curved shape of the tube was maintained.

The concentric tubes were then clamped inside the roller gear of the appropriate actuation unit, and commanded to move to one of three desired target locations. The targets were chosen to test the ability of the device to drive all degrees of freedom and reach distinct locations within the workspace of the given concentric tube set. The base, tip, and backbone positions were collected using the tracked surgical pointer, shown in Fig. 10, and a pivot calibration method was used to determine a mapping from the tip of the tracked surgical pointer to the actual sensor being tracked by the electromagnetic tracking system [22].

B. Experimental Results

The concentric tube robot was driven toward each target a total of three times and was retracted back to its original position in between each of these trials. The position of the final configuration of the concentric tube robot was measured with the tracked surgical pointer. The target and tip locations, along with smoothed backbone data (obtained by fitting a fifth order polynomial), are shown in Fig. 11.

The error between the actual measured tip position and the desired target location was calculated for each of the trials. The mean error was less than 2 mm for each target. These results demonstrate the ability of the actuation system to precisely drive a concentric tube robot to various target locations with sufficient accuracy for our particular clinical application, nonlinear renal access to kidney stones in pediatric patients. This application requires reaching targets that are on average 12.7 mm in length [23]. In the future, we plan to implement backlash compensation similar to [24] by commanding small rotations equivalent to the backlash distance. For clinical implementation, closed-loop control of the tip position could be based on external sensing or imaging of the robot tip. Teleoperation by a human operator could also reduce errors [13].

V. Applications of Handheld Device

There are several applications where surgeons and patients could benefit from having a compact, lightweight, minimally invasive actuation and control system. In general, the

surgeon can easily reorient the device and gain access to difficult-to-reach places. For example, Fig. 12(a) shows the device attached to an arm of the da Vinci Research Kit (dVRK). Previous researchers have worked to develop novel end effectors for the dVRK, including a snake-like dexterous manipulator [25] and a concentric tube instrument [26]. While these tools easily integrate with the system by using the standard da Vinci instrument disk-driven adaptor, they are limited to four degrees of freedom. By using the lightweight actuation system shown here, we propose that higher-degree-of-freedom flexible instruments could be developed.

In addition, the compact, lightweight design allows for easy mounting on a bedside arm as shown in Fig. 12(b). This standard mounting technique, while possible with some of the existing actuation designs, can be difficult to reorient due to the large size and weight. We created a vacuum-formed outer shell to house the device, and designed a 3D printed handle that can be used for easy repositioning. This same shell can be used to make the device truly handheld, as shown in Fig. 12(c) and (d). Having a handheld device would allow the surgeon to access hard to reach places within the body from any angle. It could also enable the surgical workflow to remain very similar to conventional procedures. In order to make an even more compact version of our system, we envision using the tubes themselves for the transmission. The waffle-like pattern would be integrated into the distal ends of the tubes, as shown in Fig. 13, and would be used for the translation and rotation. This would significantly reduce the overall footprint, and we leave this advancement for future work. While [27], [28] showed the development of handheld steerable devices, they are both limited to an outer stiff cannula and a single inner stylet. A handheld version of our actuation system would enable a more highly dexterous steerable device. Giving the human the ability to manually maneuver the base of the robotic device poses interesting control questions that we leave for future work.

VI. Conclusion

In this letter, we presented the design and evaluation of a compact, modular actuation and control system for flexible medical robots. We demonstrated its ability to repeatably drive a set of concentric tubes to a given target and showed its potential as a handheld device. This design is a step towards using flexible medical robots in patient- and procedure-specific applications.

This compact design facilitates maneuverability of the system during a procedure, as well as a large reachable workspace within the body. It also enables the development of multi-arm systems, in which each arm could be reoriented and repositioned over the patient. New control algorithms would need to be developed to account for purposeful human movement in combination with robotic actuation during operation. This system also prompts the need for the design of novel, ungrounded teleoperation interfaces that are intuitive for controlling a dexterous manipulator.

Acknowledgments

This work was supported in part by the National Institutes of Health through R01 EB018849 and in part by the National Science Foundation Graduate Research Fellowship.

The authors would like to thank Joey Greer for his help with the experimental setups and motor control, and Grant Kadokura for contribution to the device concept.

References

1. Burgner-Kahrs J, Gilbert HB, Granna J, Swaney PJ, Webster RJ III. Workspace characterization for concentric tube continuum robots," in. Proc IEEE/RSJ Int Conf Intell Robots Syst. 2014:1269–1275.
2. Baykal C, Torres LG, Alterovitz R. Optimizing design parameters for sets of concentric tube robots using sampling-based motion planning," in. Proc IEEE/RSJ Int Conf Intell Robots Syst. 2015:4381–4387.
3. Morimoto TK, Greer JD, Hsieh MH, Okamura AM. Surgeon design interface for patient-specific concentric tube robots," in. Proc Int Conf Biomed Robot Biomechatronics. 2016:41–48.
4. Morimoto TK, Okamura AM. Design of 3-D printed concentric tube robots. IEEE Trans Robot. Dec; 2016 32(6):1419–1430.
5. Webster RJ III, Jones BA. Design and kinematic modeling of constant curvature continuum robots: A review. Int J Robot Res. 2010; 29(13):1661–1683.
6. Webster RJ III, Okamura AM, Cowan NJ. Toward active cannulas: Miniature snake-like surgical robots," in. Proc IEEE/RSJ Int Conf Intell Robots Syst. 2006:2857–2863.
7. Sears P, Dupont P. A steerable needle technology using curved concentric tubes," in. Proc IEEE/RSJ Int Conf Intell Robots Syst. 2006:2850–2856.
8. Swaney PJ, et al. Design of a quadramanual robot for single-nostril skull base surgery," in. Proc ASME Dyn Syst Control Conf. 2012:387–393.
9. Burgner J, et al. A telerobotic system for transnasal surgery. IEEE/ASME Trans Mechatronics. Jun; 2014 19(3):996–1006.
10. Su H, et al. A MRI-Guided concentric tube continuum robot with piezoelectric actuation: A feasibility study," in. Proc IEEE Int Conf Robot Autom. 2012:1939–1945.
11. Comber DB, Barth EJ, Webster RJ III. Design and control of an magnetic resonance compatible precision pneumatic active cannula robot. ASME J Med Devices. 2014; 8(1) Art. no. 110 031.
12. Burgner J, et al. An autoclavable steerable cannula manual deployment device: Design and accuracy analysis. ASME J Med Devices. 2012; 6(4) Art. no. 410 071.
13. Burgner J, Swaney PJ, Lathrop RA, Weaver KD, Webster RJ III. Debulking from within: A robotic steerable cannula for intracere-bral hemorrhage evacuation. IEEE Trans Biomed Eng. Sep; 2013 60(9):2567–2575. [PubMed: 23649131]
14. Zhu Y, Swaney PJ, Godage IS, Lathrop RA, Webster RJ III. A disposable robot for intracerebral hemorrhage removal," in. Proc Des Med Devices Conf. 2016:020952-1–2-020952.
15. Slocum, AH. Precision Machine Design. Dearborn, MI, USA: Soc. Manuf. Eng; 1992.
16. Tadakuma K, et al. Omnidirectional driving gears and their input mechanism with passive rollers," in. Proc IEEE/RSJ Int Conf Intell Robots Syst. 2012:2881–2888.
17. Tadakuma R, et al. The gear mechanism with passive rollers: The input mechanism to drive the omnidirectional gear and worm gearing," in. Proc IEEE Int Conf Robot Automation. 2013:1520–1527.
18. Gilbert, HB., Rucker, DC., Webster, RJ, III. Concentric Tube Robots: State of the Art and Future Directions. Berlin, Germany: Springer; 2016. p. 253-269.
19. Much, J. MS thesis. Dept. Comput. Sci., Technische Univ. Munchen; Munich, Germany: 2008. Error classification and propagation for electromagnetic tracking.
20. Lock J, Dupont P. Friction modeling in concentric tube robots," in. Proc IEEE Int Conf Robot Autom. 2011:1139–1146.
21. Gilbert HB, Webster RJ III. Rapid, reliable shape setting of superelastic nitinol for prototyping robots. IEEE Robot Autom Lett. Jan; 2016 1(1):98–105. [PubMed: 27648473]
22. Yaniv Z. Which pivot calibration? Proc SPIE. 2015; 9415 Art. no. 941527.

23. El-Assmy A, El-Nahas AR, Abou-El-Ghar ME, Awad BA, Sheir KZ. Kidney stone size and hounsfield units predict successful shockwave lithotripsy in children. Urology. 2013; 81(4):880–884. [PubMed: 23395121]
24. Gebler D, Holtz J. Identification and compensation of gear backlash without output position sensor in high-precision servo systems," in. Proc IEEE Conf Ind Electron Soc. 1998; 2:662–666.
25. Coemert S, et al. Integration of a snake-like dexterous manipulator for head and neck surgery with the Da Vinci research kit," in. Proc Hamlyn Symp Med Robot. 2016:58–59.
26. Francis P, et al. Concentric tube instrument for the Da Vinci platform," in. Proc Hamlyn Symp Med Robot. 2016:54–55.
27. Ebrahimi R, Okazawa S, Rohling R, Salcudean SE. Hand-held steerable needle device. Proc Med Image Comput Comput-Assisted Intervention. 2003:223–230.
28. Graves CM, Slocum AH, Gupta R, Walsh CJ. Towards a compact robotically steerable thermal ablation probe," in. Proc IEEE Int Conf Robot Autom. 2012:709–714.

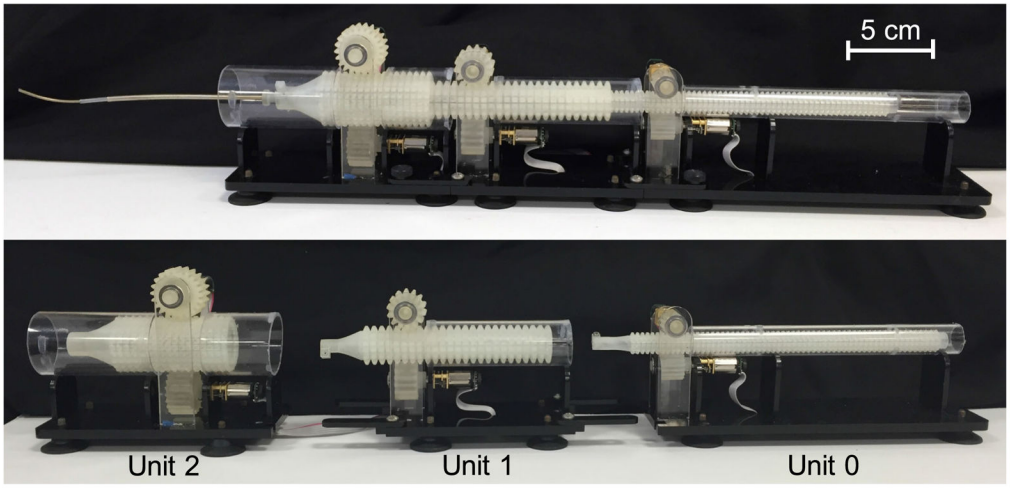

Fig. 1.
Modular actuation and control system shown holding three concentric tubes (top) and separated into individual actuation units (bottom).

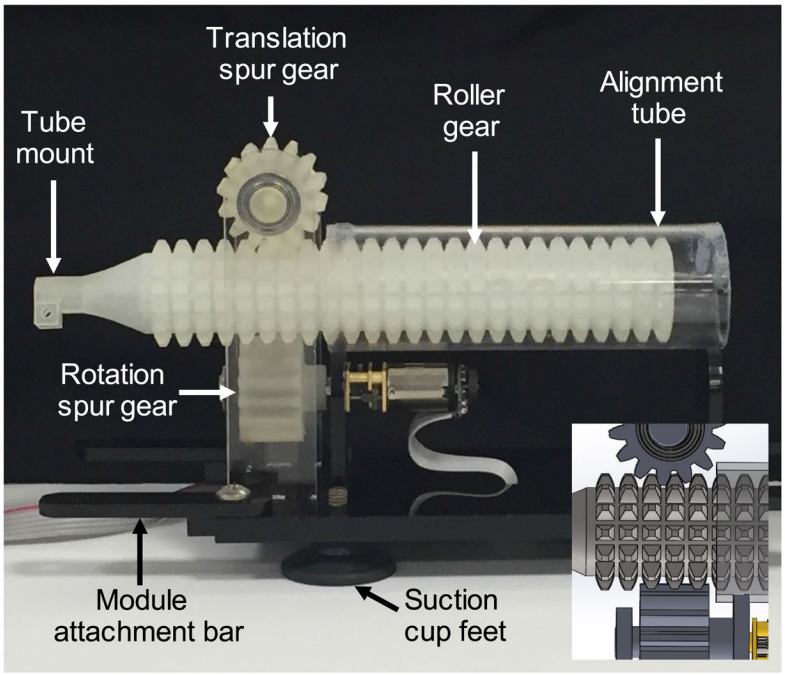

Fig. 2.

Single actuation unit module used to drive one concentric tube. Each module includes a roller gear with a mount for the concentric tube, a translation spur gear, a rotation spur gear, a tube to maintain axial alignment, suction cup feet for securing the unit to the table, and bars to attach the units together. Inset image shows closeup rendering of roller gear.

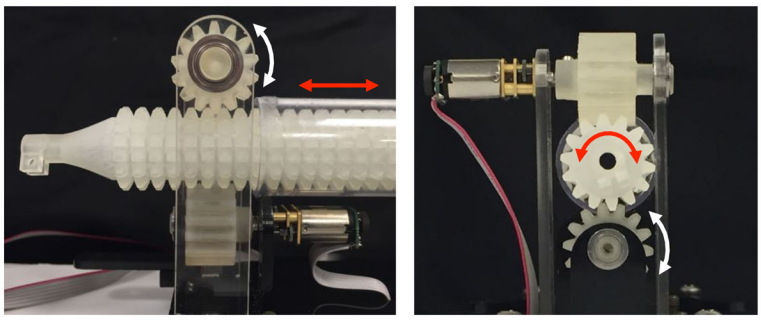

(a) (b)

Fig. 3.

Actuating the (a) translation spur gear allows insertion and retraction as the teeth of the spur gear interact with the axial teeth of the roller gear. Actuating the (b) rotation spur gear allows bidirectional rotation about the axis of the roller gear as its radial teeth interact with those of the rotation spur gear.

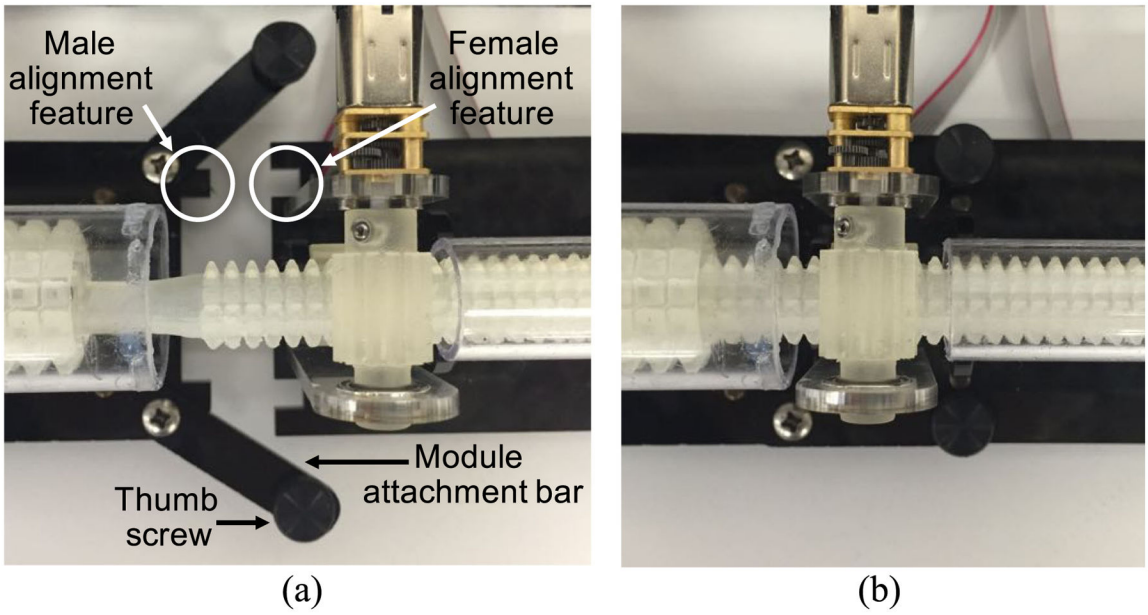

Fig. 4.
Overhead view of the alignment features and module attachment bars (a) before connecting two actuation units and (b) after.

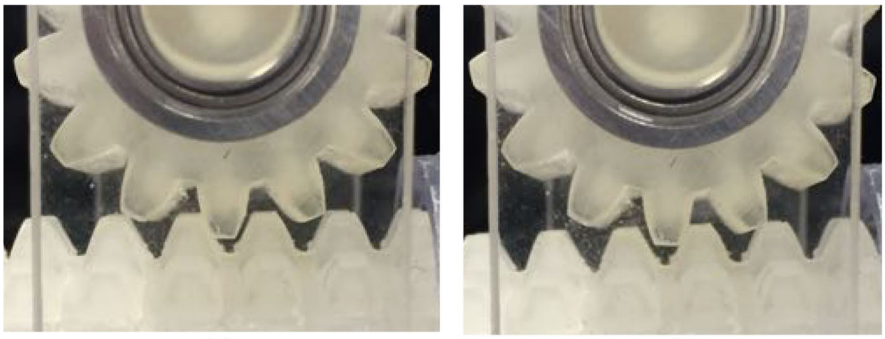

Fig. 5.
Closeup of the (a) initial position and the (b) final position of the roller gear during a backlash experiment.

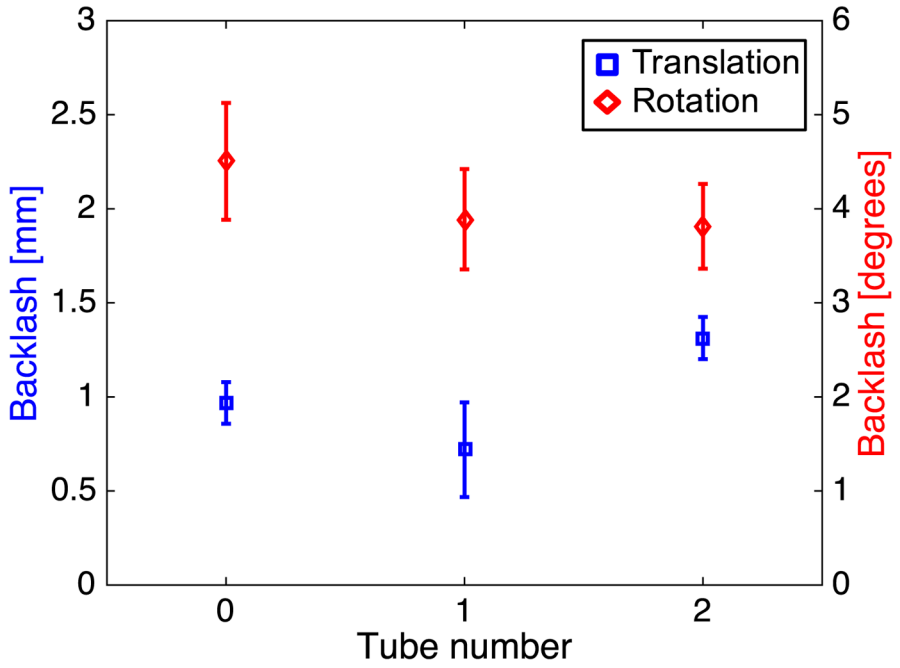

Fig. 6.

Results of backlash experiments for the translational (blue □) and rotational (red ◇) degrees of freedom for each actuation unit.

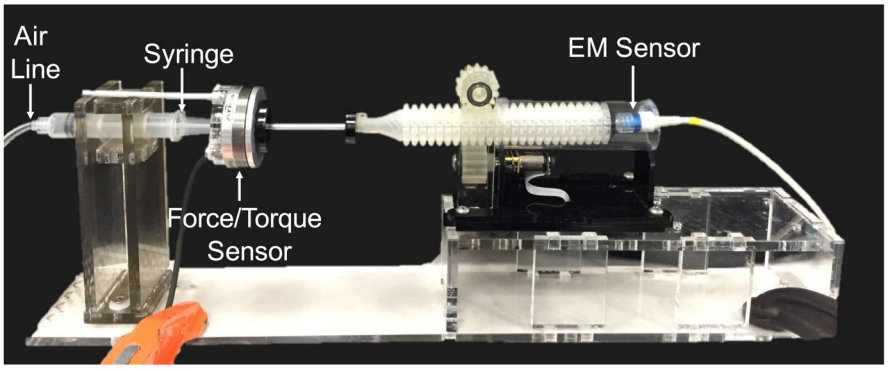

Fig. 7.

Setup for testing the translational accuracy under various loading conditions. The opposing force is provided by varying the amount of air pressure to the syringe shown. The force and position are measured with the Mini 45 force/torque sensor and EM tracker (not shown), respectively.

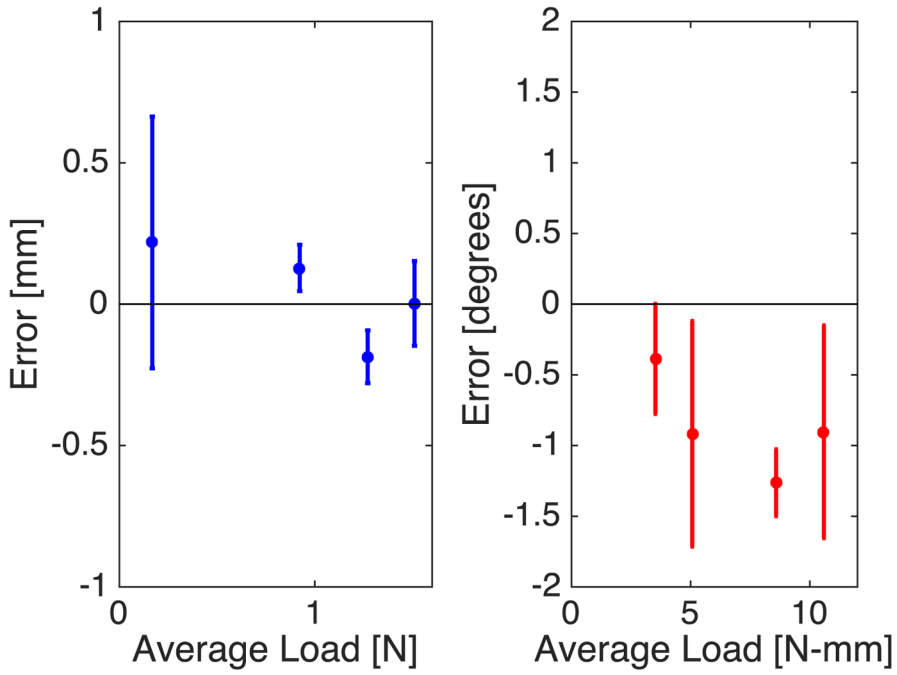

Fig. 8.
Translational (left) and rotational (right) accuracy under various loading conditions.

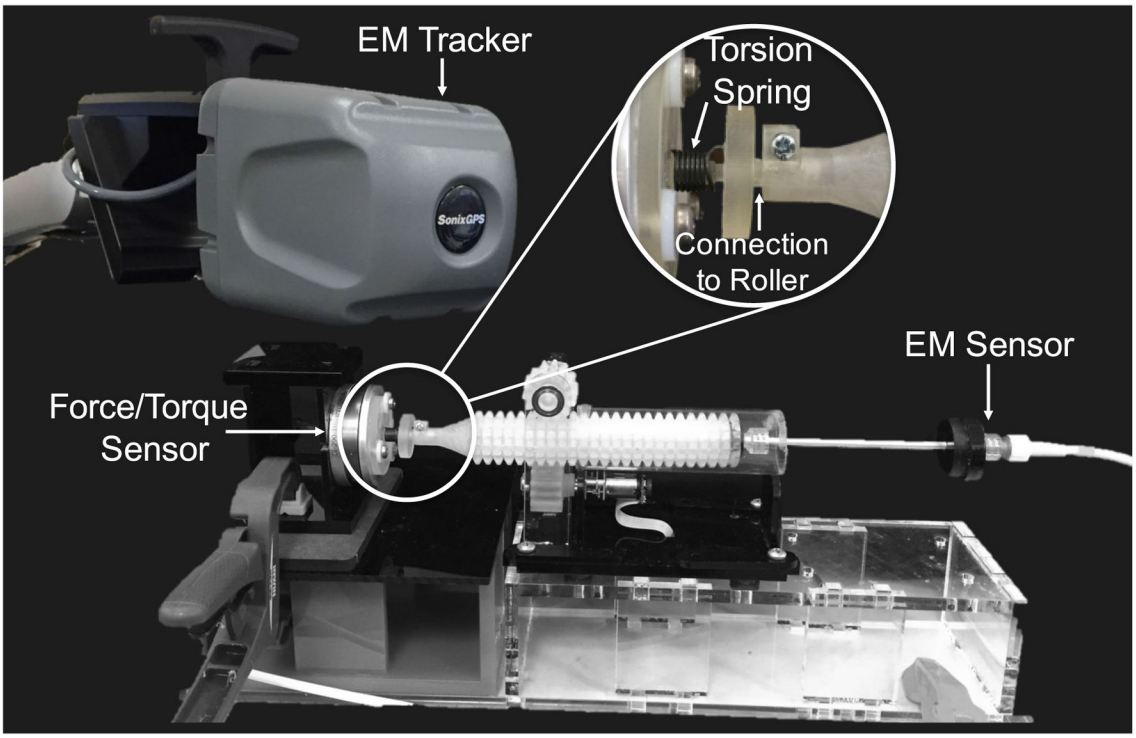

Fig. 9.

Setup for testing rotational accuracy under various applied torques that are provided by a torsion spring. A force/torque sensor measures the torque as the actuation unit is commanded to rotate against the torque of the spring.

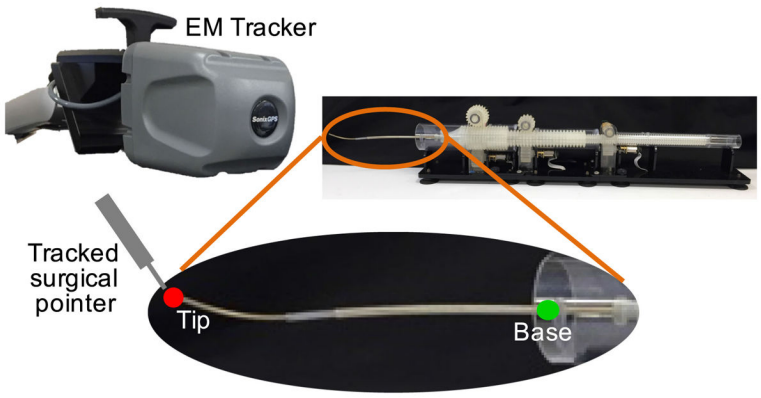

Fig. 10.

Setup for measuring the concentric tube robot position to determine the error between the actual tip position and the desired target location.

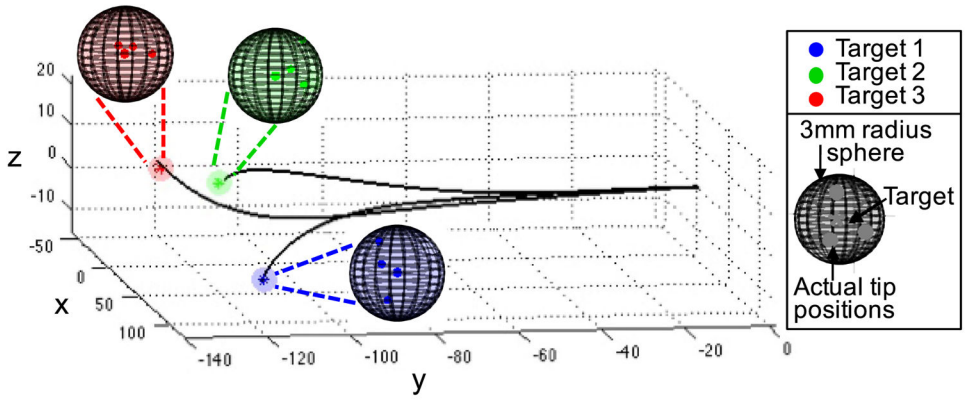

Fig. 11.

Smoothed backbone data showing the general shape of the concentric tube robot, along with the target locations and actual final tip positions.

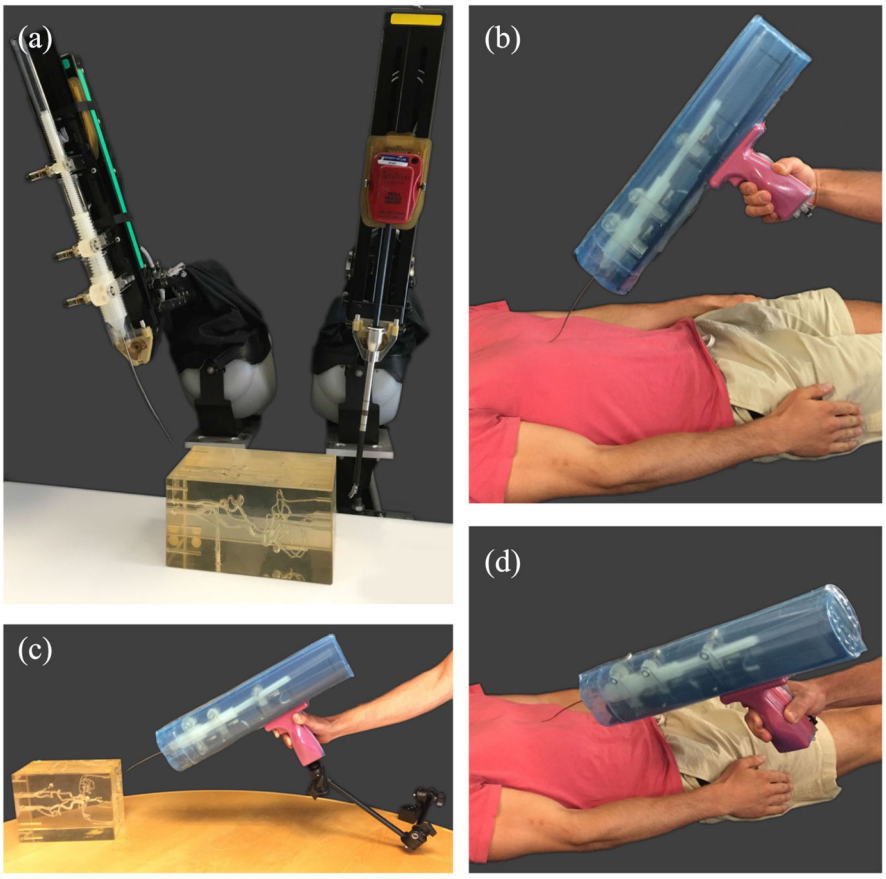

Fig. 12.

Three potential use cases include (a) mounting the device to the arm of the dVRK (da Vinci research kit), (b) mounting to a bedside arm where the handle can be used to reorient, and (c) and (d) being truly handheld and easily repositioned by the user.

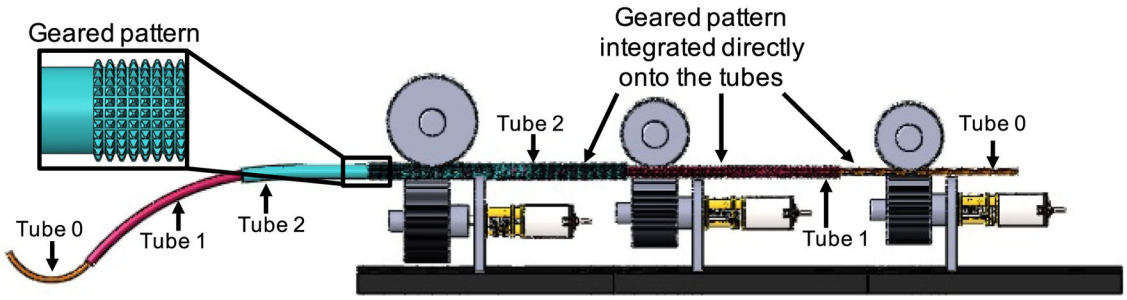

Fig. 13.

Future version of the system where the waffle-like pattern is integrated into the distal ends of the tubes, enabling the tubes themselves to be used as the transmission.

TABLE I

Design Specifications

	Roller Gear		Translation Spur Gear		Rotation Spur Gear		Entire Unit		
Module #	**Pitch Diameter [mm]**	**Teeth #**	**Pitch Diameter [mm]**	**Teeth #**	**Pitch Diameter [mm]**	**Teeth #**	r_{trans}/r_{roll}	r_{rot}/r_{roll}	**Translation Distance [mm]**
0	12	12	12	12	16	16	1	1.3	182
1	21	14	21	14	21	12	1	1	110
2	32	25	28.16	22	25.6	20	0.88	0.8	64

IEEE Robot Autom Lett. Author manuscript; available in PMC 2018 June 01.

TABLE II

Tube Parameters

Tube Num	*OD* [mm]	*ID* [mm]	$[mm^{-1}]$	L_c	L_s
0	1.514	0.902	0.0222	38	268
1	2.543	1.829	0.0060	42	137
2	3.226	2.896	0.0062	50	50